Dry season circulation-type classification applied to precipitation and temperature in the Peruvian Andes

DRY SEASON CIRCULATION TYPE CLASSIFICATION APPLIED TO PRECIPITATION AND TEMPERATURE IN THE PERUVIAN ANDES

M. BONSHOMS[a], F. J. ALVAREZ-GARCIA[b], J. UBEDA[a], W. CABOS[b], K. QUISPE[c], G. LIGUORI[d]

[a] *Departamento de Geografía. Universidad Complutense de Madrid*

[b] *Departamento de Física y Matemáticas. Universidad de Alcalá de Henares*

[c] *Servicio Nacional de Meteorología e Hidrología de Perú*

[d] *ARC Centre of Excellence for Climate Extremes, School of Earth, Atmosphere and Environment, Monash University, Melbourne, Australia*

ABSTRACT

We present the first systematic classification of circulation regimes that characterize the Tropical Andes during the dry season (May-August). We apply the hierarchical k-means clustering method to ERA-Interim reanalysis data of daily mean geopotential height at 500-hPa and 200-hPa levels for the period 1981-2015. Specifically, by combining the variability in intensity and location of geopotential anomalies we identify 12 Circulation Types (CTs). We then establish the relationship between the CTs and surface conditions in the Peruvian Andes (PA) analysing high-resolution gridded datasets of daily mean temperature and rainfall. Our results indicate that intense precipitations and low minimum temperatures are often associated with an Upper Tropospheric Trough (UTT) centred at subtropical latitudes (~30°S) and between 80°W to 70°W of longitude. Moreover, drier and warmer conditions across the entire PA region are largely associated with 3 anticyclonic CTs. Strong negative anomalies in daily maximum (minimum) temperatures can be related to the effect of day (night) cloudiness in the radiative balance, but also to subtropical cold air advections favoured by the UTT. While CTs featuring warmer (colder) conditions have become more (less) frequent in the last decades of the record, there is no systematic link between positive or negative trends in occurrence and the wetter and drier character of the CTs. The annual frequencies of 10 CTs are significantly correlated with El Niño-Southern Oscillation, with warmer and drier (cooler and wetter) CTs generally preceded by an El Niño (La Niña) in the previous wet season.

Key words: *Andes, Circulation types, K-means, Precipitation, Temperature, Tropics*

This article has been accepted for publication and undergone full peer review but has not been through the copyediting, typesetting, pagination and proofreading process which may lead to differences between this version and the Version of Record. Please cite this article as doi: 10.1002/joc.6593

*Correspondence to: M. Bonshoms Calvelo. *Research Group in Physical Geography of High Mountains. Department of Geography. Complutense University of Madrid, C/ Profesor Aranguren, Ciudad Universitaria, 28040 Madrid, Spain. E-mail: martibon@ucm.es*

1. INTRODUCTION

Around 86% of Peruvian population is settled in the productive valleys of the extremely arid Pacific coast and the semi-arid Andean region (INEI 2018). Population growth and economic activities in these areas (irrigated agriculture, hydropower, industry, mining, etc.) impose an increasing water demand, which is critically dependent on Andean freshwater supply. During the Wet Season (WS), the hydric requirements are satisfied by precipitation in the Andes. Nevertheless, during the Dry Season (DS), the freshwater availability largely hinges on glacial melting runoff, resources from the few existing reservoirs, as well as on occasional Andean precipitation. Besides, during the DS, cold outbreaks and snowfalls in the Peruvian Andes (PA) also cause severe socio economic impacts in population health, agriculture and road communications.

Circulation Type classifications (CTCs) are a powerful tool for identifying recurrent patterns in atmospheric variability. They have been used in a wide variety of contexts, such as the evaluation of long-term changes in atmospheric circulation (Kyselý and Domonkos, 2006; Lorenzo *et al.*, 2011), analysis of extreme weather events like heat or cold episodes (Kyselý and Huth, 2008), floods (Prudhomme and Genevier, 2011), droughts (Richardson *et al.*, 2018) or even lightning activity (Ramos *et al.*, 2011), among many others. CTCs were developed until the 70's, using mostly sea level pressure (SLP) data (e.g. Lamb, 1972; Hess and Brezowsky, 1952). The propagation of new automatic methodologies and the use of multiple databases, motivated the harmonization of CTCs through the European project COST 733 (Philipp *et al.*, 2010). A thorough review of CTCs can be found in Ramos *et al.* (2015). Many works have addressed the relation between CTCs and rainfall (Maheras *et al.*, 2018; Bartoszek and Skiba, 2016; Jacobeit *et al.*, 2017), temperature (Maheras *et al.*, 2006; Kyselý and Huth, 2008), or both variables (Jacobeit *et al.*, 2009; Vallorani *et al.*, 2018). Some works analyse the impact of the CTs in different high mountain areas like the Pyrenees (Esteban *et al.*, 2005), the Alps (Masson and Frei, 2014; Panziera *et al.*, 2015) or the Himalayas (Zhang, Chen and Yao, 2018). However no such attempt has yet been made for the tropical Andes. In southern South America, Compagnucci and Salles (1997) defined 11 synoptic types for the 1972-1983 period, based on the application of Principal Component Analysis (PCA) to sea level pressure data. Solman and Menéndez (2003) applied the k-means method to daily 500-hPa geopotential height data from the NCAR/NCEP reanalysis. For the same region, Bischoff and Vargas (2003) analysed Weather Types Circulations considering

geopotential heights at 500 and 1000 hPa, evaluating their relation with extreme climatic conditions. More recently, Penalba *et al.* (2013) elaborated a CTC using an Unrotated Principal Component Analysis (T-mode) and the k-means method on the SLP over an extended region of the central-southern South America. The CTs obtained were related to the rainfall in the southern La Plata Basin. For the Amazon basin, a CTC based on 850-hPa wind data, combining artificial neural network and Hierarchical Ascendant Classification, was related to rainfall variability (Espinoza *et al.*, 2012). Chaves and Cavalcanti (2002) analysed the circulation patterns over a large area including South America and the Pacific and Atlantic Oceans. They found a strong relation between the position of the Bolivian High and the Northeastern Brazilian Vortex and rainfall variability in a region located in the south of northeastern Brazil. Rainfall in the tropical region of the eastern South America is also related to El Niño-Southern Oscillation (ENSO) phases due to the displacement of the Walker circulation. Except for these 2 works on the tropical South America (Espinoza *et al.*, 2012; Chaves and Cavalcanti, 2002), most of the research in this line has been focused on the extratropics. Furthermore, no specific investigation has been made for the tropical Andes, as pointed out previously, in spite of its socio-economic and ecological relevance.

This work addresses variability in the Peruvian Andes during the DS. The main objective is to gain insight into the circulation patterns that governing temperature and precipitation variability in the PA. To achieve this objective the following specific steps are taken:

- To obtain a CTC focused on PA for the DS of the 1981-2015 period.
- To determine circulation patterns that modify significantly precipitation and temperature in the PA, especially those related to precipitation and cold outbreak episodes.
- To inspect the trends in the annual frequencies of CTs, and to identify their relationship with ENSO phases.

The study is organized as follows. The climatic characteristics of the PA and the CTC domain are presented in section 2. The methodology and data used are described in section 3. In section 4, results and discussions of the obtained CTs, their statistical characteristics, and their relation with PA thermal and pluviometric anomalies, as well as to ENSO indices, is presented. Finally, conclusions are exposed in section 5.

2. STUDY AREA

2.1 The Peruvian Andes and its climatic characteristics

We define the Peruvian Andes (PA) as the continuous region above 3000 meters above sea level (masl) extending from 6°S to 18°S latitude within the territory of Peru. This highland tropical region runs parallel to the South America Pacific coast for about 1400 km, with altitudes peaking higher than 6000 masl. The climatic conditions are defined by a marked seasonality in cloudiness, humidity and precipitation, but low annual thermal amplitude. Subtropical thermal conditions prevail during the DS while tropical conditions are predominant during the WS (Kaser and Osmaston, 2002).

During the DS, the northward displacement of the atmospheric circulation leaves the PA under the subsiding branch of the Hadley cell and dry upper-level westerlies linked to the Subtropical Jet Stream. Moreover, the Bolivian High, an anticyclonic system at ~200 hPa (Lenters and Cook, 1997), is deconfigured and displaced northwards (Figure 2, bottom). The absence of cloudiness and the predominantly dry atmospheric conditions increase the daily thermal amplitude (Sarmiento, 1986) and minimum temperatures can descend below 0°C at 3000 masl and -20°C above 4000 masl (SENAMHI, 2010).

During the WS (Figure 2, top), the Subtropical Jet Stream is displaced southwards, while the Bolivian High determines the moisture advection and upper-level divergence, triggering convection over the Tropical Andes (Vuille and Keimig, 2004; Falvey and Garreaud, 2005; Garreaud, 2009; Garreaud *et al.*, 2009a). Fluctuations in zonal winds have been related to the moisture transport variability at the diurnal (Reuder and Egger, 2006; Garreaud *et al.*, 2009a), intraseasonal (Garreaud and Garreaud, 2000; Falvey and Garreaud, 2005) and interannual (Garreaud *et al.*, 2001; Garreaud, *et al.*, 2003; Vuille and Keimig, 2004; Segura *et al.*, 2016) time scales. At the interannual time scale, climate variability is also affected by the El Niño Southern Oscillation (ENSO) (Garreaud, 2009; Barsugli and Sardeshmukh, 2002; Ding *et al.*, 2014; Ciasto *et al.*, 2015).

Based Sagredo and Lowell (2012) we classified the PA in 4 sub-regions taking into account the mean October precipitation (PPOct) and the difference in mean December/July temperature (ΔT) (Table 1).

2.2 Circulation Type Classification Domain

The ability of CTC techniques to capture patterns with relevance on local surface conditions strongly depends on the choice of the domain size. In this respect, Beck et al. (2016) showed that domain sizes with a horizontal dimension of approximately 1300–1800 km (in the zonal direction) include most frequent size ranges of synoptic scale systems and present the highest skill in relating surface conditions to circulation systems. This must be large enough to capture

synoptic-scale systems, but limited to those that directly influence the climatic conditions of the analysed domain. However, due to the large extension of the target area, as well as to cope with its tropical characteristics, we adopt a slightly wider horizontal dimension (~2100 km) than suggested by Beck et al. (2016). The domain used to perform the CTC comprises an area located in the western tropical South America, covering from 5°S-25°S and from 84.75°W-65.25°W. However, the circulation patterns are displayed over 0°-30°S and 95.25°W-54.75°W for a clearer illustration of their structure. The classification and the display domains, as well as sub-domains defined to locate the geopotential height anomalies are depicted in Figure 1 (left).

3. DATA AND METHODS

3.1 Data used in the classification

Bearing in mind the peculiarities of the tropical troposphere and the high altitude of the mountain range, daily (00:00 UTC) geopotential height data at the 200-hPa (Z200) and the 500-hPa (Z500) pressure levels have been used for the classification procedure. The data has been taken from the ERA-Interim reanalysis data set (Dee *et al.*, 2011), provided by the *European Centre for Medium-Range Weather Forecasts* (ECMWF). Daily data for the DS within the period 1981-2015, on 0.75° X 0.75° horizontal regular grid, have been processed. We consider the DS as the 123-days period from 1 May to 31 August, as proposed by Sicart *et al.* (2011) and Rabatel *et al.* (2013). Because we intend to explore changes in the frequency of CTs possibly reflecting the global warming trend, no detrending has been applied to the data.

3.2 Surface data sets

A gridded data sets provided by the Servicio Nacional de Meteorología e Hidrología de Perú (SENAMHI) have been used to evaluate the impact of CTs on surface conditions for the 1981-2015 period. The Peruvian Interpolated data of the SENAMHI's Climatological and hydrological Observations (PISCO) products are 0.5º horizontal resolution gridded daily precipitation and maximum/minimum temperature. These products combines satellite information with surface observations of the SENAMHI network (Aybar *et al.* 2019).

For precipitation, PISCOp V2.1_Beta incorporate satellite rainfall from the Climate Hazards group Infra-Red Precipitation with Station data (CHIRPS) and homogenized daily rainfall observations. For maximum and minimum temperature, PISCOt V1.1 combines surface temperature data from MODIS-LST satellite and homogenized daily extreme temperatures (Huerta et al. 2017).

We have analysed the relationship between the CTs and surface conditions, defining new variables described in Table 2.

To characterize ENSO variability, commonly used Niño indices are derived from the National Oceanic and Atmospheric Administration (NOAA) Extended Reconstruction SST, version 5 (ERSST.v5) product (Huang *et al.*, 2017). ERSST.v5 consists of monthly-mean values from 1854 to the present on a 2° × 2° horizontal grid globally.

3.3 Classification method

The identification of CTs has been performed following the k-means clustering algorithm, which is a partitioning algorithm known as the dynamic cluster method based on recurrent patterns. This method was developed by MacQueen (1967) and has been applied by many authors to cluster analysis (Anderberg, 1973; Hartigan, 1975; Gordon, 1999). It has been extensively used to elaborate CTs classifications in the Northern Hemisphere (Kageyama *et al.*, 1999; Robertson and Ghil, 1999; Simonnet and Plaut, 2001) and less frequently in the Southern Hemisphere (Bejarán and Camilloni, 2003; Solman and Menéndez, 2003). The k-means method has shown a good performance against other methods in providing a good distribution of temperature and precipitation (Huth *et al.*, 2016). This method attempts to distribute the cases of a sample among several classes with a minimum degree of internal dissimilarity, measured by the sum of the squared Euclidean distances to the class centroid, given by the average of their cases. In our application of k-means, the classification procedure is initialized with centroids obtained from a preliminary hierarchical clustering of the data, in line with suggestions put forward in the literature (Steinley, 2006; Yarnal, 1993). The methodology proposed by Ward (1963) has been chosen for this step, for the sake of consistency of classification metrics with k-means.

This combined hierarchical k-means clustering method has been applied jointly to the Z500 and 200 Z200. As a previous step, a PCA was performed (in S mode) to reduce the dimensions of the sample. For each of those fields, the leading components explaining over 99% of the variance were retained and rotated using the varimax criterion. 9 components were kept for Z500, and 7 for Z200, and were merged to enter the classification procedure.

A key issue in k-means refers to the selection of the number of classes K to be established. Several elements have been taken into account in this study to this end. One of them rests on the procedure proposed by Krzanowski and Lai (1988). Their statistic (henceforth, KL statistic) essentially monitors the reduction in intra-cluster variance brought about by adding one more group, relative to that provoked by a further increment. A high score in this statistic is expected for the selected value of K. The combined Ward's hierarchical – k-means approach has been applied to the rotated set of PCA components for diverse values of K, and the KL statistic has been computed for each of

them. The first local maximum in this statistic occurs at K=2, and the ensuing ones appear at K=4, 8, 12 and 15 (values higher than K=16 were not considered, not to exceed estimates of the suitable value for our sample size, after Spekat *et al.*, 2010). Deeming K=2 a too gross division, an initial classification has been formed using K=4. This results in four groups or prototypes displaying quite distinct features, both in their circulation patterns and in their impact on weather at the surface of our target region. A refinement of this initial aggregation is then pursued by evaluating two aspects for the next maxima at K= 8, 12, and 15. The inspection of Ward's dendrogram (not shown) reveals that in the range from 8 to 15, it is K=12 that yields better defined classes in the hierarchical procedure. Additionally, we have evaluated the consistency of the finer partitions with the prototypical classification, finding again a more positive score for K=12. A classification has been then established for this number of classes. The comparison of the outcome to the previous prototypes leads to the conclusion that useful information has been gained in terms of the discrimination of impacts over the target region.

4. RESULTS AND DISCUSSION

4.1 Circulation Type Classification

A total of 4305 days from May to August (MJJA) for the 1981-2015 period, have been classified into 12 CTs, based on the combined Z500 and Z200 data. The types are denoted as C1 to C12, ranking from greater to smaller size. They are arranged by structural similarity in Figure 3, which depicts the mean Z500 and Z200 (Figure 3, A and C), their respective anomalies, hereinafter referred to Za500 and Za200 (Figure 3, B and D), and the annual frequency of each type (Figure 3, E). The anomalies correspond to deviations from the MJJA Z500 and Z200 monthly mean.

The 12 CTs can be seen to arise from variations in the location and intensity of two large-scale systems, identifiable at both levels (500 and 200 hPa):

- **Upper Tropospheric Highs (UTH)**: located over the continent at low latitudes and sustained by thermal air expansion in the continental tropical South America.
- **Upper Tropospheric Troughs (UTT)**: mainly located at subtropical latitudes and related to mid-latitude lows.

For ease of description, we have developed a nomenclature based on the prevalence of a Ridge/Trough system at Z200, located over the Ocean/Coast/Continent at Z200 and considering the intensity of geopotential height anomalies at 200 hPa. Based on the differences between absolute maximum positive and negative Za200, the CTs have been considered as described in (Table 3).

A right subscript in the capital letter indicates the location of the maximum/minimum Za200 values within the sub-domains (blue rectangles) defined in Figure 1 (left). These sub-domains extend across the following longitudes: **Ocean** (95°W-80°W); **Coast** (80°W-70°W) and **Continent** (70°W-55°W). Finally, a left superscript has been added to denote the intensity of Za200, according to the thresholds specified in Table 4. The name of each CT as well as information on the frequency of occurrence is summarized in Table 5. Although this nomenclature is based solely on the Za200 anomalies, it must be noted that it is established *a posteriori* on the basis of the classification results, and that these depend also on the information at the 500 hPa level. The discrimination between types becomes at times more evident in the Z500 level (such is the case, for instance, between C8 and C2, or C7 and C11) and this allows the classification algorithm to extract the separate features also in Z200 on which we set our nomenclature.

The configuration of circulation patterns in Figure 3 yields the following description of the different CTs:

$^{S}R_{continent}$ **(C8)**. An anticyclonic CT characterized by a strong UTH centered over the Altiplano extending a strong non-tilted ridge across Peru. An equatorial NW flow affect the northern PA favoured by the position of the UTH.

$^{W}R_{continent}$ **(C2).** An anticyclonic type displaying comparatively weak positive Za200 over the continent. At Z200, a quite intense NW flow affects the PA favoured by a short negatively tilted ridge that extends from the north of Peru to Paraguay. At 500 hPa, the UTH is centered east of Bolivia with no relevant Za500 over the study area.

$^{M}R_{coast}$ **(C1).** An anticyclonic CT similar to C8 but with lower Za200 off the Chilean coast. At 500 hPa upper-level flows are similar than in C8. However, at Z200 westerly flows affect the PA due to low Z200 values and gradient over Peru.

$^{S}T_{continent}$ **(C10).** A Cyclonic type characterized by a strong subtropical UTT located on the continent. At Z200 flows are from W-SW with a moderate intensity only in the southern part of the DOTPA. At Z500, the UTT only affects the southern extreme of the PA with westerly winds, while central and northern PA are under the influence of the intense UTH.

$^{W}T_{continent}$ / $^{W}R_{ocean}$ **(C4).** A Mixed type with a quite intense anticyclone at 500 hPa and warm upper level conditions at 200 hPa. At Z200 a neutrally tilted ridge extends towards the subtropical

Pacific Ocean while weak negative anomalies are located over the continent, linked to a weak trough. At Z500, all the PA are under the anticyclonic influence, with not well defined flows.

$^{W}T_{ocean}$ / $^{W}R_{continent}$ **(C3).** A Mixed type with a weak intensity of the oceanic trough and the continental ridge. In this type, the trough and the ridge are further west and southward than in the previous CT. At 500 hPa, the UTT is also westward located and less northward extended with a predominance of the UTH over Peru. Flows at 500 hPa run parallel to the mountain range.

$^{S}T_{coast}$ **(C5).** A Cyclonic type with strong Za200 centered in front of the Chilean coast and extended along the coast of Peru. At Z200 and Z500, the southern PA sits under the influence of the divergent sector of the deep UTT. In the southern PA, a NW flow prevails while light western flows dominate in the north, at both analysed levels.

$^{M}T_{coast}$ / $^{W}R_{continent}$ **(C9).** A Mixed type with a moderate UTT over the coast and a weak but extended ridge that covers all the continental sector of the study area. At 500 hPa, the presence of a UTT at subtropical latitudes together with the UTH over the Amazon basin, favours a NW flow over the central-southern PA. At 200 hPa, NW flows affect the entire PA.

$^{VS}T_{ocean}$ **(C12).** A Cyclonic type characterized by the presence of a UTT over the Subtropical Pacific Ocean, with strong Za200. The Amazonian UTH with close to neutral geopotential values is centered east of Bolivia. In combination with the UTT, a relatively humid northwestern flow is canalized along the PA.

$^{VS}T_{continent}$ **(C11).** A Cyclonic type similar to C10 but with lower geopotential heights over the continent where negative Za200 and Za500 prevail. At 500 hPa, a weakened UTH, located over Brazil, extends a zonal ridge into the Pacific Ocean, favouring weak NE flows on the north. A UTT at the southeastern sector of the study area favours SW flows in the southern PA. At Z200, colder conditions prevail over the PA with a westerly flow in the north and SW winds in the southern PA.

$^{M}T_{continent}$ **(C7).** A Cyclonic type similar to C10 but with colder conditions at Z200 and Z500 over the PA. It is characterized by a UTT at the southeastern sector of the study area, with the center of moderate negative Za200 located over Bolivia. Cold upper-level conditions prevail favouring an intense SW zonal flow over the southern PA.

$^{W}R_{coast}$ / $^{W}T_{continent}$ **(C6).** A Mixed type featuring negative (positive) anomalies on the tropics (subtropics) resulting in a westerly flow over the PA at 200 hPa. This circulation pattern results from the remnants of the UTT once it has passed the Andean mountain range, but also from extended Atlantic UTT. At 500 hPa, the UTH is located in its seasonal position but weakened and extending a ridge to the chilean coast. Relatively moist NE flows affect the PA at Z500 while dry and cold conditions prevail at Z200.

In the next section, the impact of these CTs on thermal and pluviometric conditions at the surface of the target area is addressed.

4.2 Impact of the CTs on surface climate

4.2.1 Daily Precipitation

Considering the entire PA, C12 ($^{VS}T_{coast}$) stands out as the wettest type. It is associated with Wet to Extremely Wet conditions (according to the thresholds given in Table 6) in the central and southern PA and, with a lower intensity, in the northern PA (Figure 4). Its high values of DPR, denoting relatively intense episodes of rainfall under this CT, lead to its substantial contribution to the total precipitation (CDSP) gathered in the southern half of the PA, even in spite of its low frequency of occurrence. Type C5 displays a similar rainfall distribution, with lower DPR, yet with a wider impact on CDSP, due to its more frequent occurrence (Figure 4). Both C12 and C5 are cyclonic types ($^{VS}T_{ocean}$ and $^{S}T_{coast}$ respectively) characterized by the presence of a deep UTT at 500 and 200 hPa (Figure 3) located near the western coast of South America. Although C9 ($^{M}T_{coast}$ / $^{W}R_{continent}$) bears structural similarity to C12 and C5, the shorter latitudinal extension of the UTT axis confines positive DPR values to the southern PA, with high DPR values in their western slope. Positive DPR in extended areas of the central and southern PA are also detected with type C6 ($^{W}R_{coast}$ / $^{W}T_{continent}$). This CT, due to its relatively high frequency (f_T ~9%), has a moderate to very high CDSP in the southern PA, particularly in SDOTPA. The combination of moist NE flows at 500 hPa with dry and cold conditions at 200 hPa could contribute to enhanced convection on the mountainous areas of the southern PA, resulting in increased DPR. With C11 ($^{VS}T_{continent}$), positive Wet to Extremely Wet conditions (Table 6) stretch across the Wet PA whilst negative values occur over the Dry PA. This spatial pattern can be explained by the position of the UTT, with their divergence (convergence) sector affecting the eastern (western) PA.

Dry to Extremely dry DPR (Table 6) throughout the PA are detected under antic C8 and C1 (Figure 4). These CTs feature anticyclonic conditions ($^{S}R_{continent}$ and $^{M}R_{coast}$, respectively) characterized by strong or moderate positive Za200 centered over the continent or the coast, and a

pronounced southward expansion of the anticyclone at Z500. A pattern of negative DPR values in the southern and central PA, with neutral to moderately wet conditions to the north, appears for types C4, C10, C3. Type C7 shares this dipolar character, albeit considerably weakened. For types C4 and C10 ($^{W}T_{continent}$ / $^{W}R_{ocean}$ and $^{S}T_{continent}$, respectively), with strongly negative DPR in the south, the rainfall anomalies can be attributed to the upper level convergence over the continent, upstream of the UTT. It is worth mentioning the sharp pluviometric contrast between C10 and type C11 ($^{VS}T_{continent}$). Though they both show a nucleus of drier DPR to the south, it is considerably smaller in C11, which in turn also shows wetter conditions over the rest of the PA. This suggests a high sensitivity in the area to apparently small modifications in some circulation patterns, since C10 and C11 display several common features. They essentially differ in the intensity of the UTT, (weaker in C10), and of the northward extension of the system (more extended to the north in C11).

Weakly anticyclonic type C2 ($^{W}R_{continent}$) exhibits neutral or moderately dry DPR over the PA, but produces Moderate to Very High CDSP values (Table 6) across the domain. This is due to its comparatively high frequency (f_T 11.45%, second in rank), and to its maximum occurrence in May when some precipitation still persists in the PA (especially in the northern PA). In addition to C2, other relevant contributors to CDSP are C4 (also ranking high in frequency and with maximum occurrence in May) in the northern PA, and C5, C6, C9 and C12, in the southern PA. C1 is associated with substantial CDSP along the western fringe of the northern PA (NDOTPA), likely connected to frequent coastal winter drizzle and cloudiness extending into the western Andean slope.

For the southern PA, high CDSP are detected with C2, C12, C5, C9 and C6. In spite of High DPR values of C12 in the entire PA, the CDSP is poor in the northern region but very high in the southern PA. It can be attributed to a higher range of CTs involved in precipitation in the northern PA. These wet classes, except C6 and C2, are related to positive Tna, probably due to the radiative effect of the cloudiness but also to cold upper level air advection. Interestingly, each of these types exhibits a different signature on Txa: while C12, C5 and C6 are associated with negative Txa conditions, C9 is linked to neutral Txa. Negative Txa could also be related to the combined effect of cloudiness and cold air advection.

4.2.2 Daily minimum temperature anomaly

Some CTs produce significant Tna with different intensities and extension, in broad areas of the PA (Figure 4). The C11 is the coldest type, producing Very Cold to Extremely Cold Tna

(after the thresholds described in Table 6) in the entire PA. With smaller amplitude, Cold Tna conditions are also observed with C7 in extended areas of the PA. Types C10 and particularly C4, also lead to Cold Tna, restricted to the southern PA. These 4 CTs are characterized by an UTT over the continent (they all share the $T_{continent}$ feature). The northward extension and intensity of the UTT, with its axis along the mountain range, determines the span and amplitude of negative Tna. Negative Tna and DPR produced by these types, can be attributed to the strong upstream cold and dry air advection over the PA produced by the passage of the UTT. Type C11 captures the more extreme cold events, hence its low total frequency f_T of C11 (4.79%). Their negative trend (Figure 3, E) suggests that these extreme cold events are becoming less frequent in the PA.

Type C9 is related to Moderately Warm to Very Warm Tna (Table 6) in the entire PA, but especially in the south, where higher anomalies are registered. Positive Tna in the localized areas of the southern PA are also detected in C5 and C12. These three CTs are related to positive DPR in the south so the positive Tna could be explained by the effect of cloudiness on the night-time radiative balance, which appears to be reinforced by their opposite (C5 and, more strongly, C12) or neutral (C9) impact on Txa (Figure 4). For these types, the location of the UTT west of the continent (T_{coast} or T_{ocean} feature) prevents subtropical cold air advection from overcoming the radiative effect as in the case of type C11.

In general terms, the distribution of Tna has a greater variability than Txa (Figure 6). Besides, Tna are more intense in the southern PA, due to their higher latitude and exposure to the subtropical atmospheric variability. As described, warmer (cooler) minimum temperatures are related to the presence of an UTT on the coast (continent).

4.2.3 Daily maximum temperature anomaly

Negative Txa in broad areas of the PA have been found in C12, C11, C7, C5 and with a lesser extent and intensity in C6. These CTs are characterized by the presence of negative Za200 over Peru. Strong negative Txa can be related to the effect of an increase of cloudiness produced by tropical plumes (Knippertz, 2007) downstream of the UTT, due to a reduction of the incoming solar radiation, but also to upper level subtropical cold air advection. As discussed above, the first appears to be the case of C12 and C5, where the UTT sits west of the continent and have warm Tna consistent with the radiative mechanism, whereas the second seems to hold for C11 and C7, with the UTT over the continent and consistently cooler Tna.

Positive Txa in the four sub-regions of the PA is found in C8, C2 and C1. These anticyclonic types are characterized by an intense Z500/Z200 UTH, with positive Za500/Za200 in the coastal and continental sub-domains. The warmest Txa are detected in C8 that produces Very

Warm conditions in the Southern PA and Moderately Warm to Warm conditions in the Northern PA (again following the thresholds in Table 6). The second warmest type corresponds to C2, characterized by an eastward location of the Za200 ($^{W}R_{continent}$) with the higher Txa on the SWOTPA. In C1, a type characterized by a maximum positive Za200 located on the coast ($^{M}R_{coast}$), the higher positive Txa occurs in the SDOPTA. This may suggest a relation between the longitudinal location of the positive Za200 and their impact on positive Txa over the Wet/Dry southern PA. High positive Txa could be related to dry and cloud free conditions and positive geopotential anomalies.

The remaining CTs (C10, C4, C3 and C9) have comparatively weak impacts on daily maximum temperature, neutral conditions prevail in the PA.

Positive (negative) Txa are related to drier (wetter) conditions in the Wet PA (Figure 5). This relation remains unclear for the Dry PA, where extremely low precipitations difficult the connection between dry conditions and temperatures. Besides, the CTs related to positive (negative) Txa present an increasing (decreasing) trend in their annual frequencies along the 1981-2015 period (Figure 3, E), suggesting an upper level atmospheric warming in concordance with results obtained by Vicente-Serrano *et al.* (2017).

4.2.4 Averaged impact on the PA climatic sub-regions

The scatterplots in Figures 5 and 6, examine the relationship between the impacts of the CTs on the analysed surface variables. They represent the distribution of anomalies averaged over the four areas previously defined (Figure 1, right). When spatially integrated, anomalies in precipitation and temperature show a greater variability in the southern PA than in the northern. Precipitation anomalies are only considered for the Wet PA due to the extreme aridity of the Dry PA during the DS, where only type C12 produces low positive anomalies (not shown).

Figure 5 depicts the average Tx and Tn anomalies against precipitation anomalies (DPa) over NWOPTA and SWOPTA. A rather clear distinction emerges in the NWOPTA impacts closely following the anticyclonic, cyclonic and mixed categories of CTs. The anticyclonic types, C8, C2 and C1 lead to warm Txa and dry DPa, the cyclonic C5, C7, C11 and C12 are associated with cool Txa and wet DPa, and the mixed types C3, C4 and C9 exhibit a comparatively neutral average impact on SWOTPA. There is also a fairly sharp grading in the amplitude of impacts, discriminating the different CTs. The exceptions to this behaviour are C10, with lower impacts than the other cyclonic types, and C6, with a stronger signal. The diverse effect of C10 concerning surface conditions, relative to the structurally similar type C11, was noted above. Small differences in the intensity and location of the UTT, and in the strength of the anticyclone at the 200-hPa level seem to explain its different impact. As to C6, it has a peculiar configuration, with anticyclonic

conditions in Z500 and a zonal arrangement of negative Z200a above, which justifies its distinct impact compared to the other mixed CTs. For these two types, it is the joint consideration of the structure at the 500-hPa and at the 200-hPa levels that allows to recognize their singularities.

Turning to the Tna - DPa scatterplot for NWOTPA in Figure 5, several aspects differentiate types within the same category. On the one hand, C2 shows warm Tna, in contrast to the cold values in C8 and C1. This likely connected, as well, with the much lower negative DPa in C2, as opposed to the larger dry anomalies of C8 and C1. The cyclonic types also diverge now in their Tna, with C5 and C12 displaying warmer conditions, and C7 and C11 leading to colder Tna. For C5 ($^{S}T_{coast}$) and C12 ($^{VS}T_{ocean}$), with the UTT axis west of the continent, the night-time radiative processes determine positive Tna. For C7 ($^{M}T_{continent}$) and C11 ($^{VS}T_{continent}$), with the trough axis over the continent, advection controls the Tna. Mixed type C9, now leaves the close to neutral impact and shows the warmer average Tna over NWOTPA.

The comparison of Txa against Tna for the NWOTPA and the SWOTPA areas in Figure 6 offers in a compact fashion the picture described above. The anticyclonic types C8, C2 and C1 correspond to warmer Txa, and are respectively associated with neutral, warm and cold Tna. Likewise, cyclonic types C5, C12, C7 and C11 all yield cooler Txa, but warmer Tna for the first two, and colder for the others. Though this pattern essentially holds for the scatterplot in SDOTPA, it is somewhat modified for the NDOPTA area, where cyclonic types C5 and C12 lose their cold Tna (Figure 6). In the SDOTPA region, the impact of types C4 and C10 becomes more clearly separated, both leading to colder Tna, but to respectively warm or cold Txa. In all four regions considered, the signal of type C12 is seen to be related to the coldest Txa and the wettest DPa in the 4 sub-regions of the PA. In general terms, positive (negative) Txa are linked to negative (positive) DPa, especially in the Wet PA where DPa differences between CTs are more evident (Figure 5).

Overall, the CTs are found to leave a distinct imprint on precipitation and temperature anomalies over the region of interest, with peculiarities in their distribution and intensity that can be traced back to different features in the circulation patterns, thus supporting the established classification.

4.3 CTs frequency

The annual frequency (f_A) of the CTs has been analysed for the 1981-2015 period (Figure 3, E). A well-defined positive trend is detected in the anticyclonic types C2, C8, and C1, characterized by a strong and southward displacement of the UTH at 500-hPa and 200-hPa, and connected with warm and dry conditions over the PA. On the other hand, well-defined negative

trends are observed for C6, C7 and C11. From these circulation patterns, C11 and C7 produce negative Txa in all the PA, while C6 does so in extended areas of the SWOTPA. These positive (negative) trends in the f_A of the warm (cold) types are concordant with the upper-level warming registered in recent decades in the tropics (Francou, 2003; Russell *et al.* 2017; Vicente-Serrano *et al.* 2017). No significant trends have been observed in C5, C10 and C12. Regarding CTs that produce intense negative Tna in the PA, a negative trend in the f_A of C11 and C7 points to a decrease of the coldest events.

Focusing on CTs that substantially alter daily precipitation, negative long-term trends in wet types (C12, C5, C11 and C6) and positive trends in dry types (C1 and C8), suggest that DS precipitation may have decreased in the PA over the analysed period. However, this could be partially compensated by positive trends observed for C9 (in the southern PA) or C2, with low DPR values but high CDSP. This issue deserves further attention, as precipitation, even during the DS, can play a relevant role in the mass balance of glaciers in the PA through its effect on the critical parameter of the surface albedo (Rabatel et al., 2013), and also has relevant socioeconomic implications.

The relationship among the f_A of the CTs has been analysed through the Pearson correlation coefficient (r, Figure 7). This relation may indicate the predominance of a set of clusters in a particular year, but also the daily sequence from one cluster to the next. Figure 7 highlights the strong positive correlation (r = 0.7) between C8 and C2 as well as between C2 and C9. These are the 3 types with the stronger equatorial UTH at Z200, so the strong correlation is likely arising from the continuity from one CT to the next. Actually, C2 is the most frequent CT following after C8 (83.9%), and C2 circulation patterns often evolve towards C9 (26.4%). Negative correlations are also significant (r= -0.6) between some CTs. As highlighted in Figure 7, C6 and C7 have strong negative correlation ($r \leq -0.4$) with other five types (C8, C2, C4, C9 and C10). The f_A of C6 and C7 increases during anomalously cold Pacific SST (as described in section 4.5), while CTs negatively correlated with C6 and C7 are more frequent during warm SST anomalies (SSTa) in the EPO. This indicates a strong relationship between the long-term variability of the f_A of the CTs and SSTa in the EPO.

4.4 Relationship between CTs and ENSO

The large-scale atmospheric disturbances produced during mature ENSO phases, El Niño and La Niña, distort the circulation over the Andes at different tropospheric levels, impacting on precipitation and air temperature (Vuille *et al.*, 2000; Garreaud, 2009; Rabatel *et al.*, 2013). In the PA, El Niño tends to produce dry and warm conditions, while La Niña episodes are associated with

cold and wet conditions (Rabatel *et al.*, 2013; Veettil and Kamp, 2017). It is important to mention that impacts of ENSO in the Andean precipitation anomalies has been focused on the WS.

Given ENSO's dominant role on interannual time scales, we analysed the relationship between the interannual f_A of the CTs and several commonly used ENSO indices such as Niño1+2, Niño3, Niño3.4, Niño4 (Trenberth and Stepaniak, 1997) and the Cold Tongue Index (CTI) (Deser and Wallace, 1987). Figure 8 shows the correlation between ENSO indices during the preceding Wet Season (DJFM) and the f_A of each CT.

Strong positive correlations ($r \geq 0.5$) are found between all the El Niño indices and the f_A of C9 and C2. The common characteristic of these CTs is an intensification of UTH at 200 and 500 hPa over the continent. It can respond to the expansion of tropical western South America troposphere, due to the heat transfer from the EPO. A strong positive correlation has also been observed for C8 in El Niño 4. Moderate positive correlation ($0.40 \leq r < 0.50$) is detected between SSTa in the eastern EPO and the f_A of C10 (figure 8).

On the other hand, strong negative correlation ($r \leq -0.5$) is found between different El Niño indices and the f_A of C3 and C6. Also a moderate negative correlation ($-0.50 < r \leq -0.40$) is detected for C5 in all El Niño indices except Niño 1+2, and for C11 in El Niño 1+2.

No correlation ($r \simeq 0$) has been observed between the El Niño indices and the f_A of C12, which produces the highest positive daily precipitation anomalies in the PA.

The correlation values described above show that, during the warm (cold) phases of ENSO, CTs characterized by positive (negative) upper-level geopotential height anomalies.

There is no evident relationship between ENSO phases and the f_A of circulation patterns characterized by a subtropical UTT. However, C11, which is associated with low temperatures in the PA, is negatively correlated to El Niño indices in the eastern EPO pointing to higher occurrence during La Niña. The CTs with strong correlations with ENSO have also a high correlation among their f_A (Figure 7). This may indicate a predominance of sets of CTs during positive/negative ENSO phases leading to different impacts on PA surface conditions during the DS. During the El Niño years, there is a high f_A of C9 and C2, C10 and C8 in the subsequent DS. The years of the maximum occurrence (Table 5) of C9 (1998), C2 (2015) and C10 (1983) correspond to extraordinary El Niño years in the 3.4 region, while for C8 (2010), matches with moderate El Niño, based on ONI categories. On the other hand, maximum f_A of C11 and C12, both characterized by very strong negative Za200, occurs during a weak La Niña year (1984) (Table 5) in spite of their low correlation with El Niño indices.

In general, except C4 and C12, all the CTs show statistically significant correlation with one or more SST-based ENSO indices, revealing a tight relationship between tropical Pacific SSTa and upper level CTs during the DS. Consistent with this, the signature of ENSO appears often in regression maps obtained by regressing the f_A time series of each CT onto SSTa in the Pacific basin (Figure 9). It is noteworthy that among positive ENSO-related CTs, all but C8 present regression patterns that resemble the canonical El Nino rather than the central Pacific El Nino (Capotondi et al., 2015). On the other hand, C3, C5 and C6 reveals a classic La Niña SSTa pattern (Figure 9).

In general terms, and in agreement with previous studies (Garreaud 2009; Veettil and Kamp, 2017), we found that CTs connected to positive (negative) ENSO phases lead to warmer and dry (cooler and wet) conditions on the PA. This relation is more robust for temperature than for DS precipitation.

5. SUMMARY AND CONCLUSIONS

This study presents the first systematic classification of the circulation regimes that characterize weather dynamics of the Tropical Andes. The hierarchical k-means technique has been applied to Z500 and Z200 ERA-Interim daily geopotential height data, for the Dry Seasons (MJJA) of the 1981-2015 period. Despite the low horizontal gradients in the study area, the classification procedure is capable of extracting a number of distinctive traits concerning the dominance, location and intensity of positive/negative Z500 and Z200 anomalies.

The classification into 12 groups, though it implies relatively low rates of occurrence, allows us to detect the circulation patterns conducive to more extreme impacts, and to emphasize the sensitivity of conditions over the target area to apparently small modifications in the structure of the regional atmospheric circulation.

Increased precipitation over the entire PA is related to negative Za500 and Za200 on the subtropical Southeastern Pacific, with an UTT located off the west coast of South America. Such conditions appear, with distinctive nuances, under C12, C5 and C9 defined by negative Za500/Za200 centred in the coast sub-domain (80°W-70°W). In C9, Za200 values are less extended to the north resulting in positive DPR values confined to the southern PA. The upper-level divergence downstream of the UTT induces an increase of the instability, hence favouring precipitation. Regarding trends in precipitation, CTs associated to driest conditions in the PA (C8 and C1) increased their f_A, together with a slight reduction in the occurrence of the main DPR type (C12) and C6. However, this may be offset by the rise in occurrence of types C2 and C9, associated with higher CDSP, which might explain the lack of a clear tendency in the precipitation

gathered in the region. This issue deserves further attention, as precipitation, even during the DS, can play a relevant role in the freshwater availability.

Regarding daily minimum temperature, the C11, C7, C10 and C4 are CTs are characterized by an UTT on the continent, producing negative Tna, especially in the southern PA. For daily maximum temperature, negative anomalies are detected with 4 Types (C12, C11, C7 and C5), presumably due to the effects of cold air advection, probably dominant in types C7 and C11, or to increased cloudiness, as is likely the case for types C12 and C5. Positive Txa are linked to anticyclonic circulation patterns that produce below-average daily precipitation rates (C8, C2, C1), characterized by positive Za500/Za200 in the coastal and continental sub-domains.

The f_A of most of the CTs (10 of 12), show significant correlations with ENSO indices, evincing a strong relation between SSTa in the EPO and the upper level circulation patterns over the tropical Andes. CTs positively correlated to tropical Pacific SSTa are defined by an intense UTH at 200 hPa, indicative of warming of the tropical western South America troposphere as a result of heat transfer from the EPO. In general terms, CTs connected to positive (negative) ENSO phases lead to warmer (cooler) daily temperatures, however the relationship with precipitation is unclear. A positive (negative) long-term trend on the f_A related to warm (cold) upper-level conditions is found. These positive/negative trends are concordant with the upper-level warming in the tropics and the increase of El Niño events in the EPO registered in recent decades.

The CTC presented in this study provides a valuable benchmark for the validation of climate simulations that address the evolution of conditions in the PA. Through the established impacts on local surface conditions, it also provides a tool for projecting the future evolution of climatic conditions and water resources.

Acknowledgments

This work has been developed within the framework of FONDECYT 144-2015 Research Project. We thank all the participating institutions, especially the Servicio Nacional de Meteorología e Hidrología del Perú (SENAMHI) for PISCO dataset.

REFERENCES

Anderberg, M. R. (1973) *Cluster Analysis for Applications*. Academic Press.

Aybar, C. *et al.* (2019) 'Construction of a high-resolution gridded rainfall dataset for Peru from 1981 to the present day', *Hydrological Sciences Journal*. Taylor & Francis, 0(0), pp. 1–16. doi:

10.1080/02626667.2019.1649411.

Barsugli, J. J. and Sardeshmukh, P. D. (2002) 'Global Atmospheric Sensitivity to Tropical SST Anomalies throughout the Indo-Pacific Basin', *Journal of Climate*, 15(23), pp. 3427–3442. doi: 10.1175/1520-0442(2002)015<3427:GASTTS>2.0.CO;2.

Bartoszek, K. and Skiba, D. (2016) 'Circulation types classification for hourly precipitation events in Lublin (East Poland)', *Open Geosciences*, 8(1), pp. 214–230. doi: 10.1515/geo-2016-0019.

Beck, C., Philipp, A. and Streicher, F. (2016) 'The effect of domain size on the relationship between circulation type classifications and surface climate', *International Journal of Climatology*, 36(7), pp. 2692–2709. doi: 10.1002/joc.3688.

Bejarán, R. A. and Camilloni, I. A. (2003) 'Objective method for classifying air masses: An application to the analysis of Buenos Aires' (Argentina) urban heat island intensity', *Theoretical and Applied Climatology*, 74(1–2), pp. 93–103. doi: 10.1007/s00704-002-0714-4.

Bischoff, S. A. and Vargas, W. M. (2003) 'The 500 and 1000 hPa weather circulations and their relationship with some extreme climatic conditions over southern South America', *International Journal of Climatology*, 23(5), pp. 541–556. doi: 10.1002/joc.894.

Capotondi, A., Wittenberg, A. T., Newman, M., Di Lorenzo, E., Yu, J. Y., Braconnot, P., Cole, J., Dewitte, B., Giese, B., Guilyardi, E., Jin, F. F., Karnauskas, K., Kirtman, B., Lee, T., Schneider, N., Xue, Y. and Yeh, S. W. (2015) 'Understanding ENSO diversity'. *Bulletin of the American Meteorological Society*, 96: 921–938.

Casado, M. J., Pastor, M. A. and Doblas-Reyes, F. J. (2010) 'Links between circulation types and precipitation over Spain', *Physics and Chemistry of the Earth*. Elsevier Ltd, 35(9–12), pp. 437–447. doi: 10.1016/j.pce.2009.12.007.

Chaves, R. R. and Cavalcanti, I. F. A. (2002) 'Atmospheric Circulation Features Associated with Rainfall Variability over Southern Northeast Brazil', *Monthly Weather Review*, 129(10), pp. 2614–2626. doi: 10.1175/1520-0493(2001)129<2614:acfawr>2.0.co;2.

Ciasto, L. M. *et al.* (2015) 'Teleconnections between Tropical Pacific SST Anomalies and Extratropical Southern Hemisphere Climate', *Journal of Climate*, 28(1), pp. 56–65. doi: 10.1175/JCLI-D-14-00438.1.

Compagnucci, R. H. and Salles, M. A. (1997) 'Surface Pressure Patterns During the Year Over

Southern South America', *International Journal*, 17, pp. 635–653.

Dee, D. P. *et al.* (2011) 'The ERA-Interim reanalysis: Configuration and performance of the data assimilation system', *Quarterly Journal of the Royal Meteorological Society*, 137(656), pp. 553–597. doi: 10.1002/qj.828.

Deser, C., and J. M. Wallace, 1987: El Niño events and their relation to the Southern Oscillation: 1925-1986. J. Geophys. Res., 92, 14189-14196.

Ding, H., Greatbatch, R. J. and Gollan, G. (2014) 'Tropical influence independent of ENSO on the austral summer Southern Annular Mode', *Geophysical Research Letters*, 41(10), pp. 3643–3648. doi: 10.1002/2014GL059987.

Espinoza, J. C. *et al.* (2012) 'Large-scale circulation patterns and related rainfall in the Amazon Basin: A neuronal networks approach', *Climate Dynamics*. doi: 10.1007/s00382-011-1010-8.

Esteban, P. *et al.* (2005) 'Atmospheric circulation patterns related to heavy snowfall days in Andorra, Pyrenees', *International Journal of Climatology*, 25(3), pp. 319–329. doi: 10.1002/joc.1103.

Falvey, M. and Garreaud, R. D. (2005) 'Moisture variability over the South American Altiplano during the South American low level jet experiment (SALLJEX) observing season', *Journal of Geophysical Research Atmospheres*, 110(22), pp. 1–12. doi: 10.1029/2005JD006152.

Francou, B. (2003) 'Tropical climate change recorded by a glacier in the central Andes during the last decades of the twentieth century: Chacaltaya, Bolivia, 16°S', *Journal of Geophysical Research*. John Wiley & Sons, Ltd, 108(D5), p. 4154. doi: 10.1029/2002jd002959.

Garreaud, R. *et al.* (2001) 'Interannual Rainfall Variability over the South American Altiplano', *Journal of Climate*, 14(12), pp. 2779–2789. doi: 10.1175/1520-0442(2001)014<2779:IRVOTS>2.0.CO;2.

Garreaud, R. D. *et al.* (2009a) 'Present-day South American climate', *Palaeogeography, Palaeoclimatology, Palaeoecology*. doi: 10.1016/j.palaeo.2007.10.032.

Garreaud, R. D. *et al.* (2009b) 'Present-day South American climate', *Palaeogeography, Palaeoclimatology, Palaeoecology*. Elsevier B.V., 281(3–4), pp. 180–195. doi: 10.1016/j.palaeo.2007.10.032.

Garreaud, R. D. (2009) 'The Andes climate and weather', *Advances in Geosciences*. doi:

10.5194/adgeo-22-3-2009.

Garreaud, R. and Garreaud, R. (2000) 'Intraseasonal Variability of Moisture and Rainfall over the South American Altiplano', *Monthly Weather Review*, 128(9), pp. 3337–3346. doi: 10.1175/1520-0493(2000)128<3337:IVOMAR>2.0.CO;2.

Garreaud, R., Vuille, M. and Clement, A. C. (2003) 'The climate of the Altiplano: observed current conditions and mechanisms of past changes', *Palaeogeography, Palaeoclimatology, Palaeoecology*. Elsevier, 194(1–3), pp. 5–22. doi: 10.1016/S0031-0182(03)00269-4.

Gordon, A. (1999) *Classification*. 2nd edn. Edited by Chapman & Hall/CRC Monographs on Statistics and Applied Probability.

Hartigan, J. A. (1975) *Clustering Algorithms (Probability & Mathematical Statistics)*. New York (USA): John Wiley & Sons, Inc.

Huang, B., Thorne, P.W, Banzon,V., Boyer, T., Chepurin, G., Lawrimore, J., Menne, M.J., Smith, T.M., Vose, R.S and Zhang, H (2017). 'NOAA Extended Reconstructed Sea Surface Temperature (ERSST), Version 5'. NOAA National Centers for Environmental Information. doi:10.7289/V5T72FNM .

Huth, R., Beck, C. and Kučerová, M. (2016) 'Synoptic-climatological evaluation of the classifications of atmospheric circulation patterns over Europe', *International Journal of Climatology*, 36, pp. 2710–2726. doi: 10.1002/joc.4546.

Jacobeit, J. *et al.* (2009) 'Central European prEcipitation and temperature extremes in relation to large-scale atmospheric circulation types', *Meteorologische Zeitschrift*, 18(4), pp. 397–410. doi: 10.1127/0941-2948/2009/0390.

Jacobeit, J. *et al.* (2017) 'Atmospheric circulation types and extreme areal precipitation in southern central Europe', *Advances in Science and Research*, 14, pp. 71–75. doi: 10.5194/asr-14-71-2017.

Junquas, C. *et al.* (2018) 'Understanding the influence of orography on the precipitation diurnal cycle and the associated atmospheric processes in the central Andes', *Climate Dynamics*. Springer Berlin Heidelberg, 50(11–12), pp. 3995–4017. doi: 10.1007/s00382-017-3858-8.

Kageyama, M. *et al.* (1999) 'Weather regimes in past climate atmospheric general circulation model simulations', *Climate Dynamics*, 15(10), pp. 773–793. doi: 10.1007/s003820050315.

Kaser, G. and Osmaston, H. (2002) *Tropical Glaciers*. Cambridge (UK): Cambridge University

Press.

Killeen, T. J. *et al.* (2007) 'Dry spots and wet spots in the Andean hotspot', *Journal of Biogeography*. John Wiley & Sons, Ltd (10.1111), 34(8), pp. 1357–1373. doi: 10.1111/j.1365-2699.2006.01682.x.

Knippertz, P. (2007) 'Tropical-extratropical interactions related to upper-level troughs at low latitudes', *Dynamics of Atmospheres and Oceans*, 43, pp 36-62. doi:10.1016/j.dynatmoce.2006.06.003

Krzanowski, W. J. and Lai, Y. T. (1988) 'A Criterion for Determining the Number of Groups in a Data Set Using Sum-of-Squares Clustering', *Biometrics*. International Biometric Society, 44(1), p. 23. doi: 10.2307/2531893.

Kyselý, J. and Domonkos, P. (2006) 'Recent increase in persistence of atmospheric circulation over Europe: Comparison with long-term variations since 1881', *International Journal of Climatology*, 26(4), pp. 461–483. doi: 10.1002/joc.1265.

Kyselý, J. and Huth, R. (2008) 'Relationships of surface air temperature anomalies over Europe to persistence of atmospheric circulation patterns conducive to heat waves', *Advances in Geosciences*, 14, pp. 243–249. doi: 10.5194/adgeo-14-243-2008.

Lamb, H. (1972) 'British Isles Weather types and a register of daily sequence of circulation patterns, 1861-1971', *Geophysical Memoirs*. London (UK): Meteorological Office, 116(116), p. 85pp.

Lenters, J. D. and Cook, K. H. (1997) 'On the Origin of the Bolivian High and Related Circulation Features of the South American Climate', *Journal of Atmospheric Sciences*, 64, pp. 656–677. doi: doi.org/10.1175/1520-0469(1997)054<0656:OTOOTB>2.0.CO;2.

Lorenzo, M. N. *et al.* (2011) 'Changes in present and future circulation types frequency in northwest Iberian Peninsula', *PLoS ONE*. Edited by G. J.-P. Schumann. Public Library of Science, 6(1), p. e16201. doi: 10.1371/journal.pone.0016201.

MacQueen, J. (1967) 'Some methods for classification and analysis of multivariate observations. Proceedings of the 5th Berkeley symposium on mathematical statistics and probability', in. Berkeley (USA): University of California, pp. 1, 281–297.

Maheras, P. *et al.* (2004) 'On the relationships between circulation types and changes in rainfall variability in Greece', *International Journal of Climatology*, 24(13), pp. 1695–1712. doi:

10.1002/joc.1088.

Maheras, P. *et al.* (2006) 'Circulation types and extreme temperature changes in Greece', *Climate Research*, 30(2), pp. 161–174. doi: 10.3354/cr030161.

Maheras, P. *et al.* (2018) 'Relationship between mean and extreme precipitation and circulation types over Hungary', *International Journal of Climatology*. doi: 10.1002/joc.5684.

Masson, D. and Frei, C. (2014) 'Spatial analysis of precipitation in a high-mountain region: Exploring methods with multi-scale topographic predictors and circulation types', *Hydrology and Earth System Sciences*, 18(11), pp. 4543–4563. doi: 10.5194/hess-18-4543-2014.

Panziera, L. *et al.* (2015) 'The relation between circulation types and regional Alpine climate. Part I: Synoptic climatology of Trentino', *International Journal of Climatology*, 35(15), pp. 4655–4672. doi: 10.1002/joc.4314.

Penalba, O. C., Bettolli, M. L. and Krieger, P. A. (2013) 'Surface circulation types and daily maximum and minimum temperatures in Southern la plata basin', *Journal of Applied Meteorology and Climatology*, 52(11), pp. 2450–2459. doi: 10.1175/JAMC-D-13-039.1.

Philipp, A. *et al.* (2010) 'Cost733cat - A database of weather and circulation type classifications', *Physics and Chemistry of the Earth*. doi: 10.1016/j.pce.2009.12.010.

Prudhomme, C. and Genevier, M. (2011) 'Can atmospheric circulation be linked to flooding in Europe?', *Hydrological Processes*. John Wiley & Sons, Ltd, 25(7), pp. 1180–1190. doi: 10.1002/hyp.7879.

Rabatel, A. *et al.* (2013) 'Current state of glaciers in the tropical Andes: A multi-century perspective on glacier evolution and climate change', *Cryosphere*, 7(1), pp. 81–102. doi: 10.5194/tc-7-81-2013.

Ramos, A. M. *et al.* (2011) 'Cloud to ground lightning activity over Portugal and its association with circulation weather types', *Atmospheric Research*. Elsevier, 101(1–2), pp. 84–101. doi: 10.1016/j.atmosres.2011.01.014.

Ramos, A. M., Barriopedro, D. and Dutra, E. (2015) 'Circulation weather types as a tool in atmospheric, climate, and environmental research', *Frontiers in Environmental Science*, 3. doi: 10.3389/fenvs.2015.00044.

Raziei, T. *et al.* (2013) 'Atmospheric circulation types and winter daily precipitation in Iran',

International Journal of Climatology, 33(9), pp. 2232–2246. doi: 10.1002/joc.3596.

Reuder, J. and Egger, J. (2006) 'Diurnal circulation of the South American Altiplano: Observations in a valley and at a pass', *Tellus, Series A: Dynamic Meteorology and Oceanography*. Taylor & Francis, 58(2), pp. 254–262. doi: 10.1111/j.1600-0870.2006.00168.x.

Richardson, D. *et al.* (2018) 'A new precipitation and drought climatology based on weather patterns', *International Journal of Climatology*, 38(2), pp. 630–648. doi: 10.1002/joc.5199.

Robertson, A. W. and Ghil, M. (1999) 'Large-Scale Weather Regimes and Local Climate over the Western United States', *Journal of Climate*, 12, pp. 1796–1813. doi: 10.1175/1520-0442(1999)012<1796:LSWRAL>2.0.CO;2.

Russell, A. M., Gnanadesikan, A. and Zaitchik, B. (2017) 'Are the central andes mountains a warming hot spot?', *Journal of Climate*, 30(10), pp. 3589–3608. doi: 10.1175/JCLI-D-16-0268.1.

Sagredo, E. A. and Lowell, T. V. (2012) 'Climatology of Andean glaciers: A framework to understand glacier response to climate change', *Global and Planetary Change*. doi: 10.1016/j.gloplacha.2012.02.010.

Segura, H. *et al.* (2016) 'Evidencing decadal and interdecadal hydroclimatic variability over the Central Andes', *Environmental Research Letters*. IOP Publishing, 11(9), p. 094016. doi: 10.1088/1748-9326/11/9/094016.

SENAMHI (2010) *Atlas de heladas del Perú*. Lima (Perú): Servicio Nacional de Meteorología e Hidrología.

Sicart, J. E. *et al.* (2011) 'Analysis of seasonal variations in mass balance and meltwater discharge of the tropical Zongo Glacier by application of a distributed energy balance model', *The American journal of physiology*, 116, pp. 1–18. doi: 10.1029/2010JD015105.

Simonnet, E. and Plaut, G. (2001) 'Space-time analysis of geopotential height and SLP', *Climate Research*, 17, pp. 325–342. doi: 10.3354/cr017325.

Solman, S. A. and Menéndez, C. G. (2003) 'Weather regimes in the South American sector and neighbouring oceans during winter', *Climate Dynamics*, 21(1), pp. 91–104. doi: 10.1007/s00382-003-0320-x.

Spekat, A., Kreienkamp, F. and Enke, W. (2010) 'An impact-oriented classification method for atmospheric patterns', *Physics and Chemistry of the Earth*, 35(9–12), pp. 352–359. doi:

10.1016/j.pce.2010.03.042.

Steinley, D. (2006). 'K-means clustering: a half-century synthesis'. *British Journal of Mathematical and Statistical Psychology*, 59, 1-34.

Trenberth, Kevin E., 1997: The Definition of El Niño. Bull. Amer. Meteor. Soc., 78, 2771–2777.

Vallorani, R. *et al.* (2018) 'Circulation type classifications for temperature and precipitation stratification in Italy', *International Journal of Climatology*. John Wiley & Sons, Ltd, 38(2), pp. 915–931. doi: 10.1002/joc.5219.

Veettil, B. K. and Kamp, U. (2017) 'Remote sensing of glaciers in the tropical Andes: a review', *International Journal of Remote Sensing*. Taylor & Francis, 38(23), pp. 7101–7137. doi: 10.1080/01431161.2017.1371868.

Vuille, M. and Ammann, C. (1997) 'Regional Snowfall Patterns in the High, Arid Andes', in *Climatic Change at High Elevation Sites*. Kluwer Academic Publishers, pp. 181–191. doi: 10.1007/978-94-015-8905-5_10.

Vuille, M., Bradley, R. S. and Keimig, F. (2000) 'Interannual climate variability in the Central Andes and its relation to tropical Pacific and Atlantic forcing', *Journal of Geophysical Research: Atmospheres*. John Wiley & Sons, Ltd, 105(D10), pp. 12447–12460. doi: 10.1029/2000JD900134.

Vuille, M. and Keimig, F. (2004) 'Interannual variability of summertime convective cloudiness and precipitation in the central Andes derived from ISCCP-B3 data', *Journal of Climate*. doi: 10.1175/1520-0442(2004)017<3334:IVOSCC>2.0.CO;2.

Yarnal, B. (1993) 'Synoptic Climatology in Environmental Analysis, Studies in Climatology Series', Belhaven Press, London, 195 pp.

Zhang, X., Chen, D. and Yao, T. (2018) 'Evaluation of circulation-type classifications with respect to temperature and precipitation variations in the central and eastern Tibetan Plateau', *International Journal of Climatology*, 38(13), pp. 4938–4949. doi: 10.1002/joc.5708.

Subregion of the PA	Mean precipitation October (PPOct)	Difference December/July temperature (ΔT)	Latitudinal limit
Northern Wet Outer Tropical Peruvian Andes (NWOTPA)	PPOct >30 mm	ΔT <3ºC	North of 13.5°S
Northern Dry Outer Tropical Peruvian Andes (NDOTPA)	PPOct <30 mm	ΔT <2ºC	North of 12.0°S
Southern Wet Outer Tropical Peruvian Andes (SWOTPA)	PPOct >30 mm	ΔT >3ºC	South of 12.0°S
Southern Dry Outer Tropical Peruvian Andes (SDOTPA)	PPOct <30 mm	ΔT >2°C	South of 12.0°S *

***** An isolated area at ~14.5°S where AT <2°C, has been included in this sub-region.

Table 1. Description of the criteria used to define the Sub-regions of the Peruvian Andes

Variable	units	Definition	Considerations
Daily Precipitation Rate (DPR)	%	100*(1-(mean CT daily precipitation)/(mean DS daily precipitation))	DPR measures the change (%) in daily mean precipitation computed over the elements in a given CT, relative to the DS average.
Contribution to Total Dry Season Precipitation (CDSP)	%	CDSP = 100*(CT total precipitation)/(DS total precipitation)	Relative contribution of each CT to the total DS precipitation accumulated during the period under study.
Daily Minimum Temperature Anomaly (Tna)	°C	Average departure of CT daily minimum temperature from monthly mean	Mean deviation over the elements in a given CT from the DS average of daily minimum temperature.
Daily Maximum Temperature Anomaly (Txa)	°C	Average departure of CT daily maximum temperature from monthly mean	Mean deviation over the elements in a given CT from the DS average of daily maximum temperature.
Daily Precipitation Anomaly (DPa)	mm	Average departure of CT daily precipitation from monthly mean	Mean deviation over the elements in a given CT from the DS average of daily precipitation.

Table 2. Description of the new variables defined using PISCO datasets, used to evaluate the impact of the CTs in the surface conditions over the Peruvian Andes.

CT characterization	Za200 thresholds	Capital letter	Number of CTs
Anticyclonic	(|Za200max| - |Za200min|) > 50	R	3
Cyclonic	(|Za200max| - |Za200min|) < -50	T	5
Mixed	-50 < (|Za200max| - |Za200min|) < 50	R/T or T/R *	4

***** Capital letters ordered as a function of prevalence of maximum positive (capital letter R, first) or negative (capital letter T, first) anomalies.

Table 3. Characterisation of the circulation types attending to the magnitude of their Za200 range. Types are classified as Anticyclonic, Cyclonic or Mixed.

Max. Anomaly (abs. value)	Intensity	Superscript
$40 \leq \lvert Za200 \rvert < 80$	Weak	W
$80 \leq \lvert Za200 \rvert < 120$	Moderate	M
$120 \leq \lvert Za200 \rvert < 160$	Strong	S
$\lvert Za200 \rvert \geq 160$	Very Strong	VS

Table 4. Description of the thresholds used to categorize intensity of the geopotential height anomalies.

Cluster Rank	Circulation pattern	N° days	Total Frequency f_T (%)	Month f_M max	Month f_M min	Year/s f_A max	Year/s f_A min
C1	$^{M}R_{coast}$	555	12.89	August	July	2005	1983/92
C2	$^{W}R_{continent}$	493	11.45	May	July	2015	1986
C3	$^{W}T_{ocean}$ / $^{W}R_{continent}$	471	10.94	August	May	1999	2005
C4	$^{W}T_{continent}$ / $^{W}R_{ocean}$	418	9.71	May	July	2009	1984/85
C5	$^{S}T_{coast}$	389	9.04	July	May	2004	2010
C6	$^{W}R_{coast}$ / $^{W}T_{continent}$	387	8.99	July	May	1985	1998/10/15
C7	$^{M}T_{continent}$	374	8.69	July	May	1982	1998/10
C8	$^{S}R_{continent}$	314	7.29	May	July	2010	1982/85/86/04
C9	$^{M}T_{coast}$ / $^{W}R_{continent}$	304	7.06	May	July	1998	1984/85/08
C10	$^{S}T_{continent}$	254	5.90	May	August	1983	1985/94/96
C11	$^{VS}T_{continent}$	206	4.79	July	May	1984	1998/03/06
C12	$^{VS}T_{coast}$	140	3.25	July	May	1984	1994/98/01

Table 5. Description of the CTs obtained and their main characteristics. The frequencies in the last four columns allude to: f_T = (Total number of days by cluster)*100 / Total number of days; f_M = (Total number of days in a month by cluster)*100 / Total number of days in month (entire record); f_A = (Total number of days in a year by cluster)*100 / Number of days per year.

CDSP (%)	CDSP intensity	DPR (%)	DPR Intensity	Tn,x a (ºC)	Intensity
0<CDSP≤5	Extremely Poor	-100<DPR≤-60	Dry	Tn,x a <-2.0	Extremely Cold
5<CDSP≤7.5	Very Poor	-60<DPR≤-20	Moderately Dry	-2.0≤ Tn,x a <-1.5	Very Cold
7.5<CDSP≤10	Poor	-20<DPR≤20	Neutral	-1.5≤ Tn,x a <-1.0	Cold
10<CDSP≤12.5	Moderate	20<DPR<60	Moderately Wet	-1.0≤ Tn,x a <-0.5	Moderately Cold
12.5<CDSP≤15	High	60≤DPR<100	Wet	-0.5≤ Tn,x a ≤0.5	Neutral
CDSP>15	Very High	100≤DPR<140	Very Wet	0.5< Tn,x a ≤1.0	Moderately Warm
		DPR ≥140	Extremely Wet	1.0< Tn,x a ≤1.5	Warm
				1.5< Tn,x a ≤2.0	Very Warm
				Tn,x a >2.0	Extremely Warm

Table 6. Description of the thresholds used to determine the intensities of: Contribution to the total DS Precipitation (CDSP), Relative change in Daily Mean Dry Season Precipitation (DPR) and Daily extreme temperature anomaly (Txa/Tna).

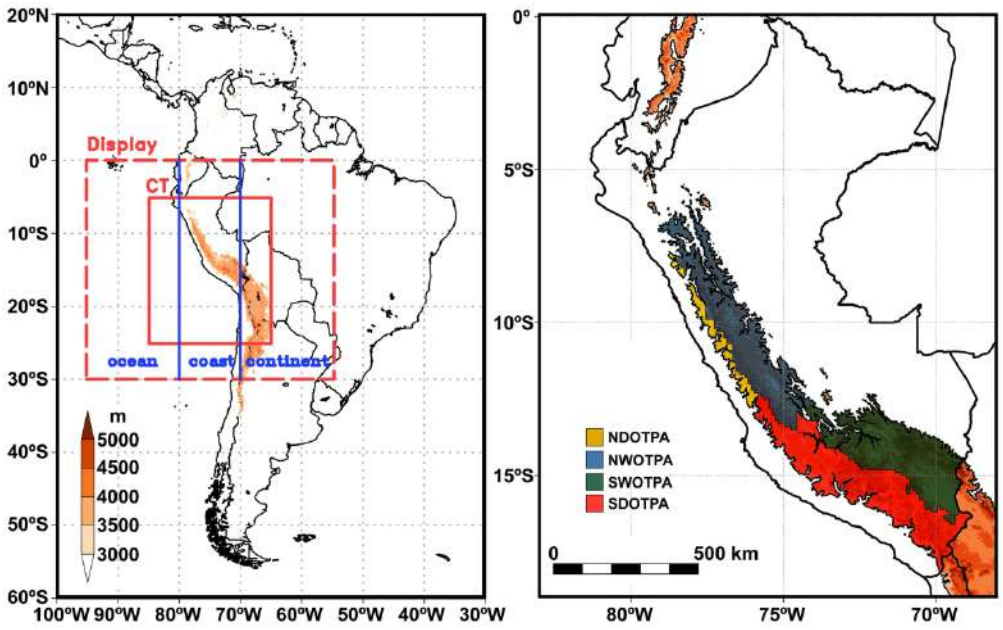

Figure 1. South America map (left) in which the CTC domain (solid red box), the domain used to display the results (dashed red box) and sub-domains used in the CTs nomenclature (blue dashed rectangles) are remarked. Map of the Peruvian Andes (right) with the 4 sub-regions. Topographic maps with the region above 3000 m highlighted to emphasize the Andes.

209x130mm (300 x 300 DPI)

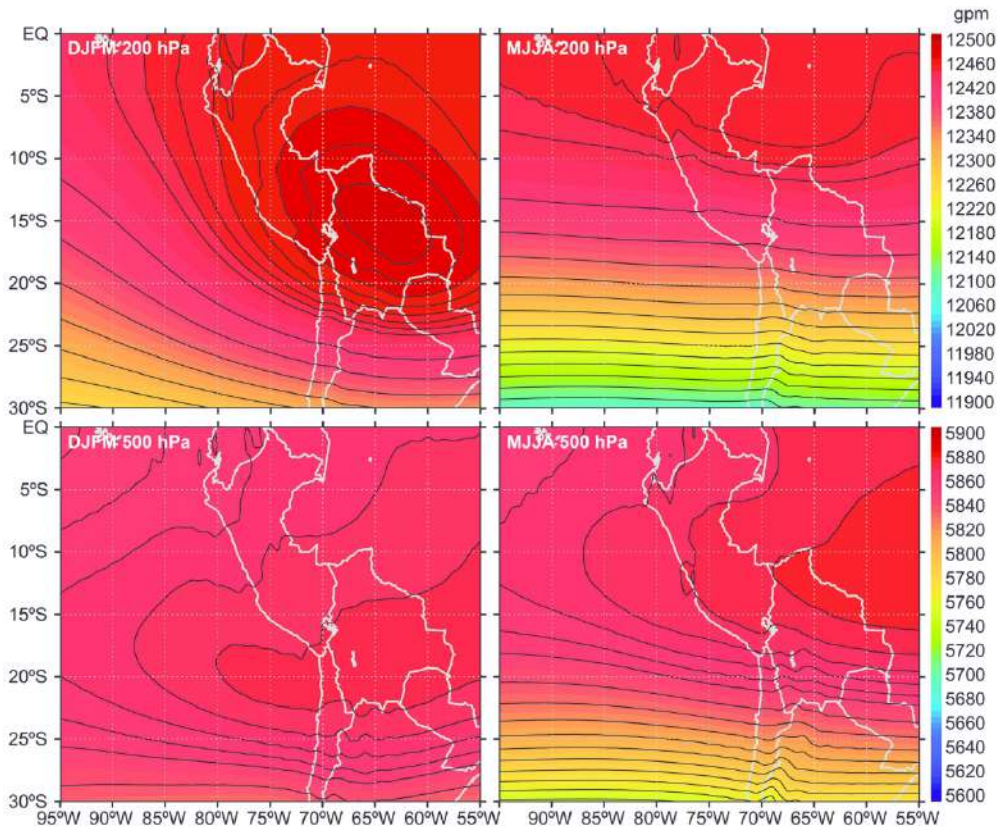

Figure 2. Mean Geopotential height at 200 hPa (top) and 500 hPa (Bottom) for the Wet Season (DJFM, left) and Dry Season (MJJA, right). Averaged Daily climatology ERAI-DACL data for the 1989-2008 period. (Janoušek 2011).

160x132mm (300 x 300 DPI)

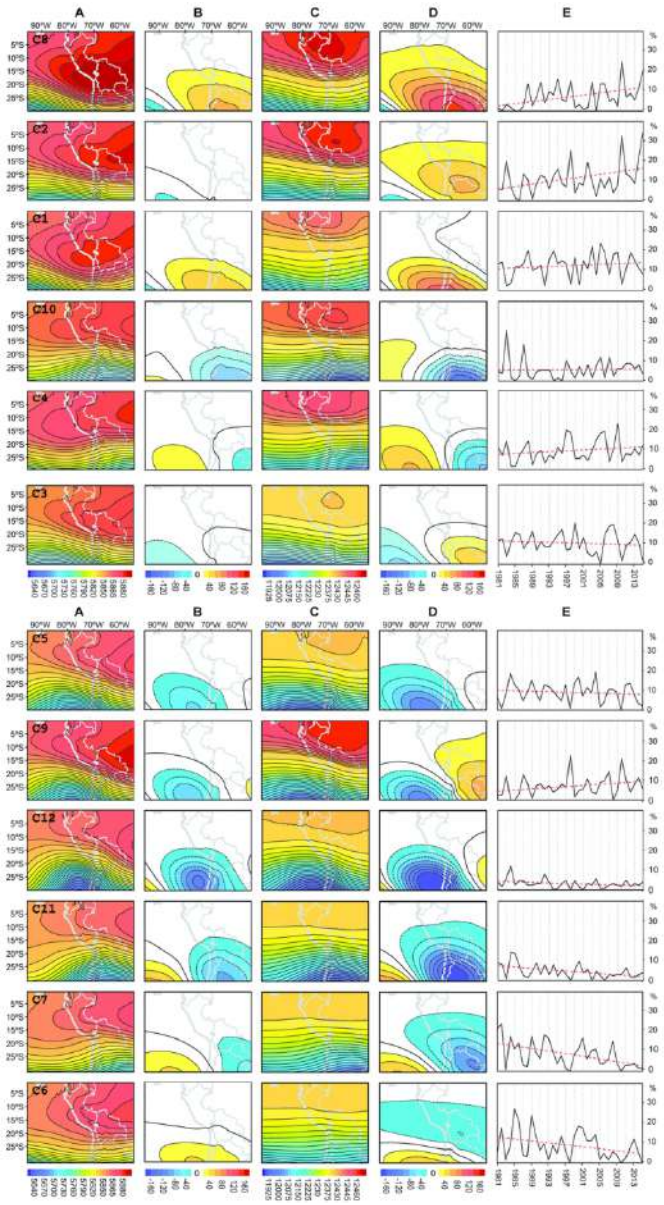

Figure 3. Geopotential height at 500 hPa (A) and 200 hPa (C) with contour and shaded interval 10/5 gpm below/over 5850 and 25/5 gpm below/over 12425 gpm. Geopotential height anomaly at 500 hPa (B) and 200 hPa (D) with 20 gpm interval. Interannual variations of the fA (%) and linear trend (red dotted line) (E). Corresponding to 12 Circulation Types for 1981-2015.

83x149mm (300 x 300 DPI)

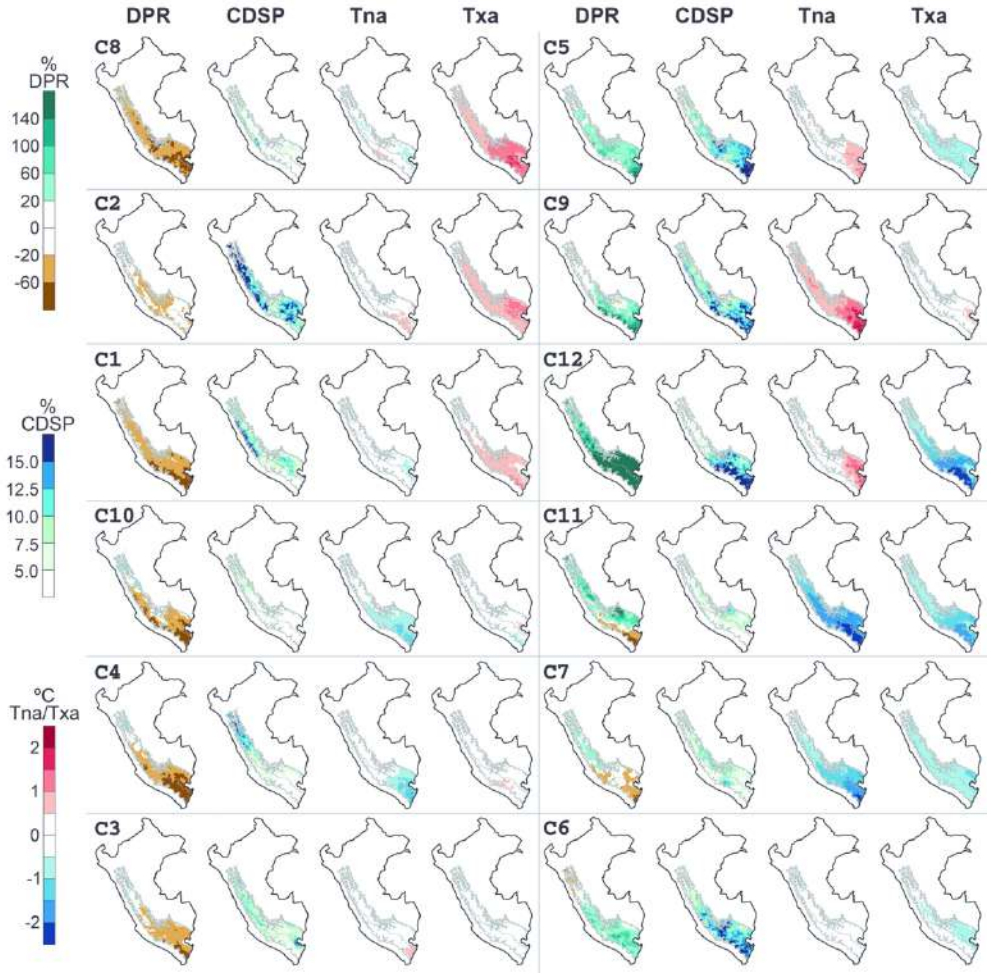

Figure 4. Relative change in Daily Mean Dry Season Precipitation (DPR), Contribution to Total Dry Season precipitation (CDSP), Minimum Temperature Anomaly (Tna) and Maximum Temperature Anomaly (Txa), corresponding to CT 1-12.

149x146mm (300 x 300 DPI)

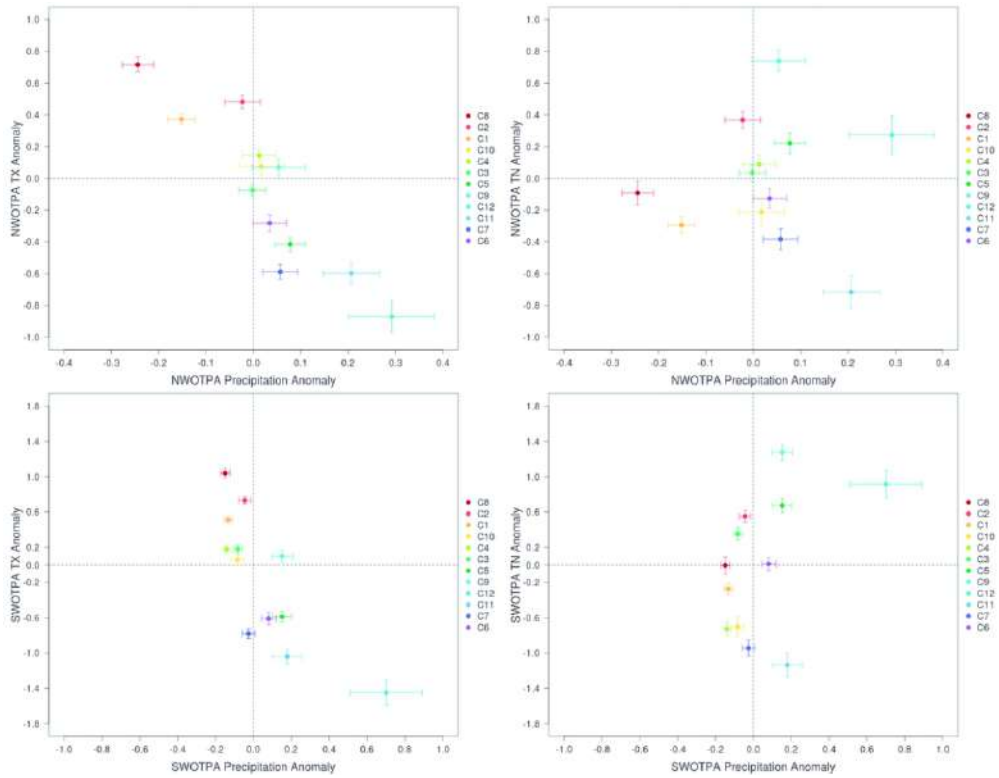

Figure 5. Scatterplots of Txa (^{0}C) and Tna (°C) against DPa (mm/d), averaged over the NWOTPA and SWOTPA regions for the 12 CTs. The dots locate the average and the bars represent the interval ±1 standard error.

99x77mm (300 x 300 DPI)

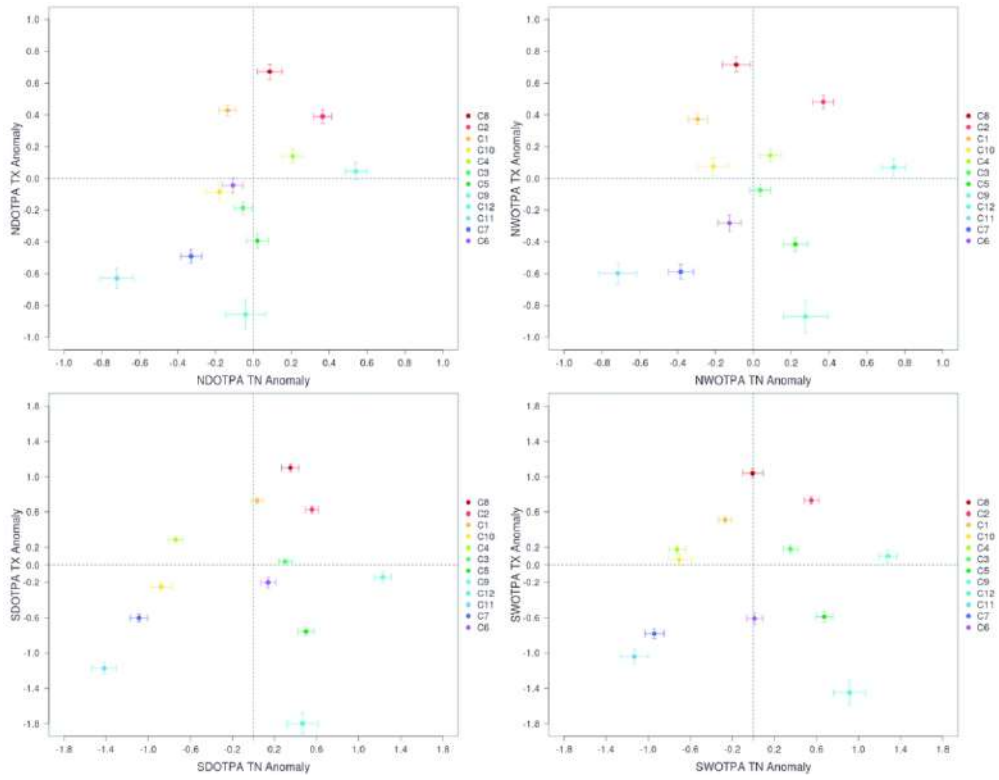

Figure 6. Scatterplots of Txa (^{0}C) against Tna (°C) averaged over the NDOPTA, NWOTPA, SDOTPA and SWOTPA regions for the 12 CTs. The dots locate the average and the bars represent the interval ±1 standard error.

99x77mm (300 x 300 DPI)

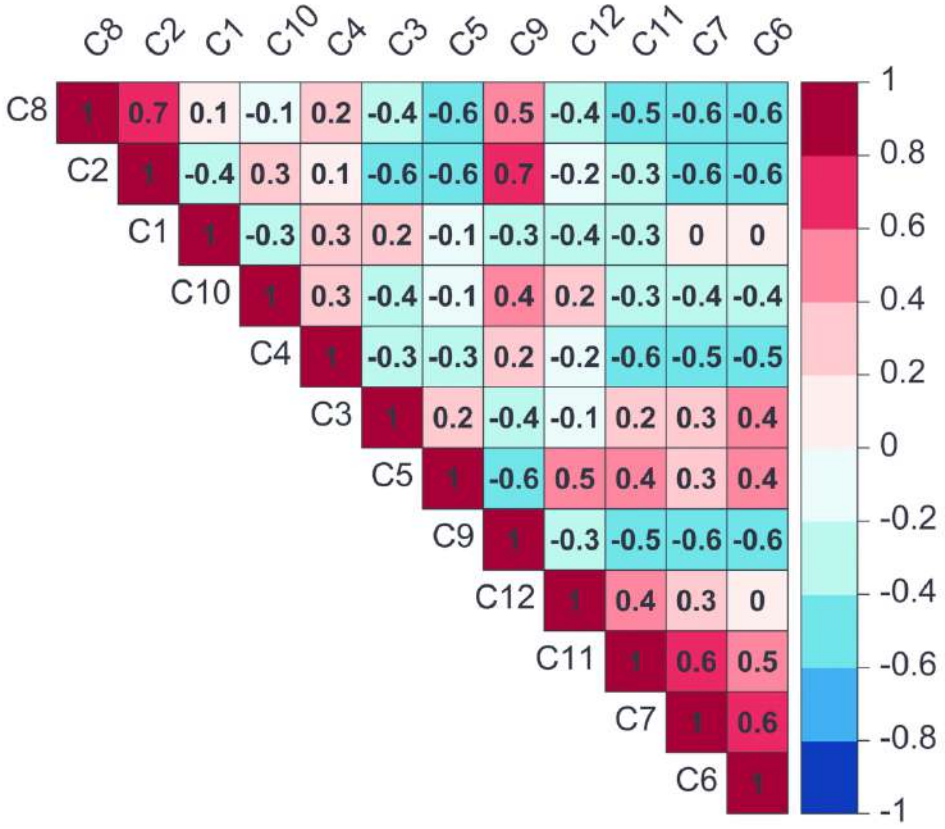

Figure 7. Correlation Coefficient (r) between the 1981-2015 annual frequencies (f_A) of the 12 CT.

149x126mm (300 x 300 DPI)

Figure 8. Correlation coefficients between the fA time series and common ENSO metrics, such as the Cold Tongue Index (CTI), Nino1+2 index, Nino3 index, Nino3.4 index and Nino4 index. These index have been averaged during ENSO peak months (DJFM) previous to analysed DS. Boldface indicates the 95% significance level based on a Student's t test.

180x65mm (300 x 300 DPI)

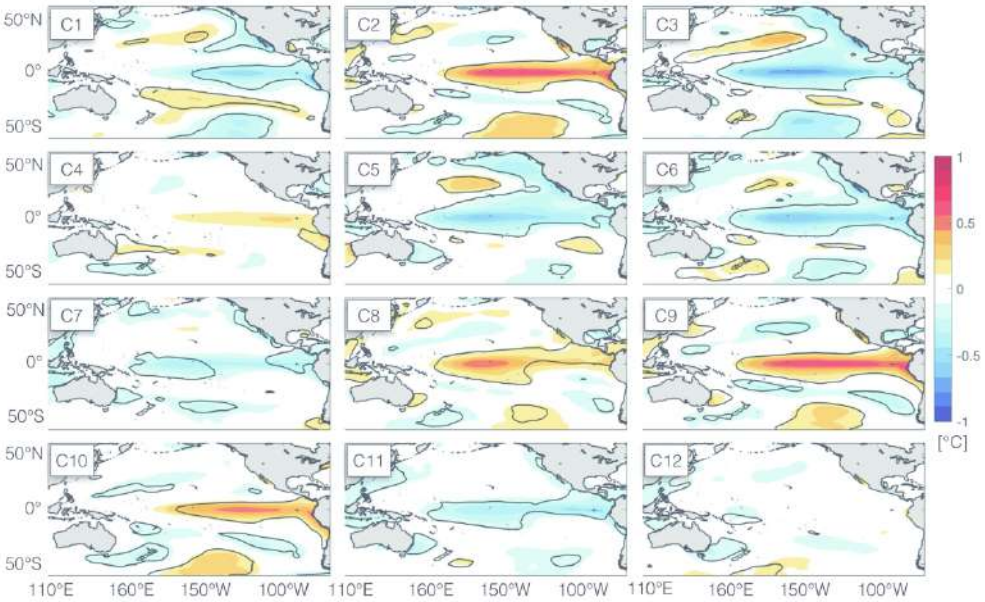

Figure 9. Regression maps between the annual CT frequency (f_A) time series and the previous DJFM SSTa. Black contours represent the 95% significance level based on a Student's t test.

199x122mm (300 x 300 DPI)